Available online at www.sciencedirect.com
ScienceDirect
International Journal of Heat and Fluid Flow 27 (2006) 967–976
International Journal of HEAT AND FLUID FLOW
www.elsevier.com/locate/ijhff

Effects of adverse pressure gradient on heat transfer mechanism in thermal boundary layer

T. Houra [a], Y. Nagano [b,*]

[a] Department of Environmental Technology, Nagoya Institute of Technology, Nagoya 466-8555, Japan
[b] Department of Mechanical Engineering, Nagoya Institute of Technology, Nagoya 466-8555, Japan

Received 9 October 2005; received in revised form 21 January 2006; accepted 4 March 2006
Available online 14 June 2006

Abstract

Characteristics of turbulent boundary layer flows with adverse pressure gradients (APG) differ significantly from those of canonical boundary layers. We have experimentally investigated the effects of APG on the heat transfer mechanism in a turbulent boundary layer developing on a uniformly heated plate. It is found that in the APG boundary layer the Stanton number follows the correlation curve for a flat plate, although the skin friction coefficient decreases drastically in comparison with zero-pressure-gradient flow. The mean temperature profiles in APG flows lie below the conventional thermal law of the wall in the fully turbulent region. Moreover, the quadrant splitting and trajectory analyses reveal that the effects of APG on the thermal field are not similar to those on the velocity field. The structural change in APG flow causes the non-local interactions between the temperature fluctuations and the wall-normal motions. However, the situation is fairly complex because the heat transport is mainly determined by the ejection motions, which are not significant contributors to the momentum transport in the APG flow.

Keywords: Turbulent boundary layer; Heat transfer; Adverse pressure gradient; Hot- and cold-wire measurement; Turbulent heat flux; Coherent structure

1. Introduction

The efficiency of industrial machinery, such as heat exchangers and turbine blades, is often restricted by the occurrence of separation due to a pressure rise in the flow direction. Therefore, it is very important to elucidate the effects of an adverse pressure gradient (APG) and establish a flow control method to avoid flow separation. In addition, the study of turbulent boundary layers subjected to a pressure gradient promises the further benefit of a deeper understanding of wall turbulence, which may not be obtained under an equilibrium zero-pressure-gradient (ZPG) condition.

For about 50 years, turbulent boundary layers with a sustained APG have been studied by many investigators. Among these previous studies, the experimental investigations conducted by Clauser (1954); Bradshaw (1967) and the theoretical one by Rotta (1962) are famous with regard to the equilibrium boundary layer (with the pressure gradient parameter kept constant), which preserves the self-similar characteristics in the flow direction. The equilibrium APG boundary layer has produced some interest in the statistical features of the self-similarity, and is thus now the subject of experiments (Skåre and Krogstad, 1994) and direct numerical simulations (DNS) (Stoke et al., 1998).

In real situations, however, the equilibrium condition is not necessarily satisfied, and the various characteristics of turbulent boundary layer flows may emerge from more general conditions. For example, the development of a turbulent boundary layer after a sudden change in external conditions (Townsend, 1976) is typical. Thus, many researchers have been investigating the boundary layers under non-equilibrium pressure-gradient conditions. Research on non-equilibrium APG boundary layers has

* Corresponding author. Tel.: +81 52 735 5325; fax: +81 52 735 5359.
E-mail address: nagano@heat.mech.nitech.ac.jp (Y. Nagano).

0142-727X/$ - see front matter © 2006 Elsevier Inc. All rights reserved.
doi:10.1016/j.ijheatfluidflow.2006.03.019

Nomenclature

B_{-vuv}, $B_{-vv\theta}$ bispectra of triple moments, $-\overline{vuv}$ and $-\overline{vv\theta}$
C_p wall static pressure coefficient, $C_p = (\overline{P} - \overline{P}_0)/(\rho \overline{U}_0^2/2)$
c_p specific heat at constant pressure
f frequency
f' dimensionless frequency, $f' = f\tau_E$
$\overline{P}$ mean pressure
P^+ dimensionless pressure gradient parameter, $P^+ = \nu(\mathrm{d}\overline{P}/\mathrm{d}x)/\rho u_\tau^3$
$\overline{P}_0$ reference inlet pressure
Pr Prandtl number
Pr_t turbulent Prandtl number
q_w heat flux at wall
R_{Δ_2} Reynolds number based on enthalpy thickness, $R_{\Delta_2} = \overline{U}_e \Delta_2/\nu$
R_{δ_2} Reynolds number based on momentum thickness, $R_{\delta_2} = \overline{U}_e \delta_2/\nu$
St Stanton number, $St = q_w/(\rho c_p \overline{U}_e \overline{\Theta}_e)$
T temperature
$\overline{T}_e$, $\overline{T}_w$ ambient and wall temperatures
t time
$\overline{U}$ mean velocity in x direction
$\overline{U}_e$ free-stream velocity
$\overline{U}_0$ reference inlet velocity
u, v fluctuating velocity components in x and y directions
u_τ friction velocity, $u_\tau = \sqrt{\tau_w/\rho}$
x, y, z streamwise, wall-normal and spanwise coordinates
y^+ dimensionless distance from wall, $y^+ = u_\tau y/\nu$

Greek symbols
α_t eddy diffusivity for heat transfer
β Clauser pressure gradient parameter, $\beta = (\delta_1/\tau_w)\mathrm{d}\overline{P}/\mathrm{d}x$
Δ thickness of thermal boundary layer
Δ_2 enthalpy thickness of thermal boundary layer
δ thickness of momentum boundary layer
δ_1, δ_2 displacement and momentum thicknesses of boundary layer
$\overline{\Theta}$ temperature difference from wall, $\overline{\Theta} = \overline{T}_w - \overline{T}$
$\overline{\Theta}^+$ temperature difference normalized by friction temperature, $\overline{\Theta}^+ = \overline{\Theta}/\theta_\tau$
$\overline{\Theta}_e$ temperature difference between wall and ambient, $\overline{\Theta}_e = \overline{T}_w - \overline{T}_e$
θ fluctuating temperature difference, $\theta = \Theta - \overline{\Theta} = \overline{T} - T$
θ_τ friction temperature, $\theta_\tau = q_w/(\rho c_p u_\tau)$
ν kinematic viscosity
ν_t eddy diffusivity for momentum transfer
ρ density
τ_E Taylor time scale or Eulerian dissipation time scale, $\tau_E = \sqrt{2\overline{u^2}/\overline{(\partial u/\partial t)^2}}$
τ_w wall shear stress

Subscripts and superscripts
0 reference inlet point
$\overline{(\ )}$ time mean value
$\overline{(\ )}_i$ fractional contribution of ith quadrant motion
$(\ )^+$ normalization by inner variables (u_τ,ν)
$(\hat{\ })$ normalization by r.m.s. value
$(\tilde{\ })$ Fourier transform
$(^*)$ complex conjugate
$\langle\ \rangle$ ensemble-averaged value

been conducted both experimentally (Samuel and Joubert, 1974; Nagano et al., 1998; Houra et al., 2000) and numerically (Spalart and Watmuff, 1993; Na and Moin, 1996; Coleman et al., 2003). The effects of an APG on compressible turbulent boundary layers are also important issues as well as the case of incompressible flows (see Fernando and Smits, 1990; Spina et al., 1994).

From our previous experiments on APG turbulent boundary layers (Nagano et al., 1998; Houra et al., 2000), we obtained the following results: (1) the standard log-law velocity profile for a ZPG boundary layer does not hold in APG boundary layers; (2) the near-wall distribution of r.m.s. velocity fluctuations cannot scale with the wall parameters; (3) the response time of turbulence to the imposed APG, which relates closely to the redistribution process of turbulent kinetic energy, differs among the streamwise, wall-normal and spanwise velocity components; (4) time scales of fluctuating velocity components, especially in the near-wall region, increase with an increase in the pressure gradient parameter; and (5) the contributions from the ejection motions significantly decrease, whereas those from sweeps increase drastically.

With respect to the investigation into the thermal fields in the turbulent boundary layer, it is still unresolved whether or not the heat transfer in APG flows is enhanced, though it is crucial in order to design high-performance heat exchangers with small drag. From the viewpoint of turbulence modeling, Bradshaw and Huang (1995), Volino and Simon (1997) have discussed the behavior of the thermal field in the APG turbulent boundary layer. They pointed out that the velocity law of the wall is more robust under streamwise pressure gradients than is the thermal law of the wall, although the energy equation does not contain the pressure-gradient-related term. They have investigated such important behavior of the APG thermal boundary layer by using the conventional mixing-length model and the two-equation turbulence model based on the equilibrium APG flow data (e.g., Blackwell et al., 1972). Therefore,

it is very important to elucidate the effects of more realistic (non-equilibrium) APG on the heat transfer in order to improve existing turbulence models and/or theory.

In the present study, we have experimentally investigated the effects of non-equilibrium APG on a turbulent thermal boundary layer developing on a uniformly heated plate with a specially devised triple-wire probe, consisting of two symmetrically bent V-shaped hot-wires (Hishida and Nagano, 1988a,b) and a fine cold-wire. We attempt to clarify the relationship between the velocity and thermal fields with quadrant splitting (Lu and Willmarth, 1973), trajectory analyses (Nagano and Tagawa, 1995), and bispectrum measurement of turbulent transports (Nagano and Houra, 2002).

2. Experimental apparatus

The experimental apparatus used is the same as described in our previous studies (Nagano et al., 1998; Houra et al., 2000). For the heat transfer experiment, a flat plate, on which an air-flow turbulent boundary layer develops, is constructed with the 2-mm thick copper plate and a.c. heated from the back of the plate. The wall temperature distribution is monitored through embedded thermocouples and kept uniform during the experiment. The test section is composed of the heated flat-plate and a roof-plate to adjust pressure gradients (see Nagano et al., 1998). The aspect ratio at the inlet to the test section is 13.8 (50.7 mm high × 700 mm wide). Under the present measurement conditions, the free-stream turbulence level is below 0.1%. To generate a stable turbulent boundary layer, a row of equilateral triangle plates is located at the inlet to the test section as a tripping device. The important flow parameters are listed in Table 1. In the APG flow, the pressure gradient dC_p/dx keeps a nearly constant value of $0.6\ m^{-1}$ over the region $65\ mm \leqslant x \leqslant 700\ mm$, and then decreases slowly (x is the streamwise distance from a tripping point). The pressure gradient parameter normalized by inner variables P^+ and the Clauser parameter β increase with increasing x, thus yielding moderate to strong APG. The Reynolds number increases with increasing x even in ZPG flows. However, the effect of the Reynolds number on turbulent flows is small compared with that of APG (Nagano et al., 1993). Thus, the following discussion is based on the variation in P^+. In order to neglect buoyancy effects, the temperature difference between the wall and ambient fluid is kept at about 10 K, which is sufficiently

Table 1
Flow parameters ($\overline{U}_0 = 10.8$ m/s, $\overline{\Theta}_e = 10$ K)

x (mm)	$\overline{U}_e$ (m/s)	δ (mm)	Δ (mm)	R_{δ_2}	R_{Δ_2}	P^+	β
935 (ZPG)	10.8	19.9	21.0	1620	1920	0	0
535 (APG)	9.1	16.2	19.4	1330	1160	0.91×10^{-2}	0.77
735 (APG)	8.3	24.6	25.3	1930	1280	1.93×10^{-2}	2.19
935 (APG)	7.6	34.2	37.1	2730	1730	2.56×10^{-2}	3.95

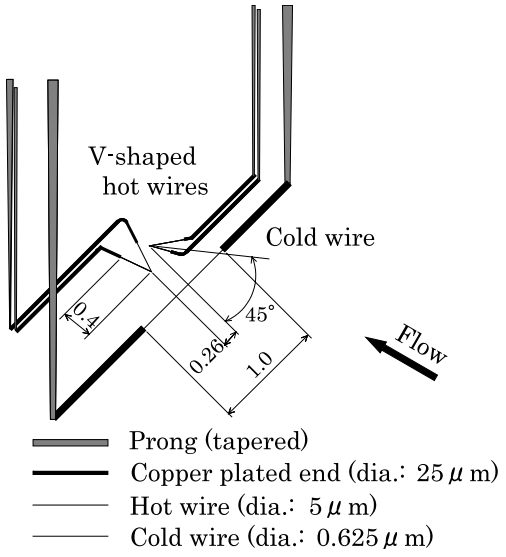

Fig. 1. Three-wire probe consisting of two symmetrically bent V-shaped hot-wires and I-shaped cold wire (all dimensions are in millimeters).

resolved by using a low-noise high-gain instrumentation amplifier and a 14-bit A/D converter. The variation in the wall temperature along the measurement length is within ± 0.5 K of the mean.

Mean velocity and mean temperature were measured with a hot- and cold-wire probe, respectively. Velocity and temperature fluctuations were simultaneously measured by the specially devised hot- and cold-wire technique (Hishida and Nagano, 1978, 1988a,b). As shown in Fig. 1, the probe consisted of three fine wires: the upstream wire serving as the constant current cold-wire (platinum 90%/rhodium 10%; diameter 0.625 μm; length 1.0 mm ≃ 18 in wall units; length-to-diameter ratio is 1600) and the two symmetrically bent V-shaped hot-wires (tungsten; diameter 5 μm; length 0.8 mm). The spatial resolution of the three-wire probe in the wall-normal direction is about 0.3 mm. The first measurement point is located at 0.6 mm from the wall, after examining reliability of the data (Tagawa et al., 1992; Nagano and Tsuji, 1994).

3. Results and discussion

3.1. Statistical characteristics

Fig. 2 shows the skin friction coefficient and the Stanton number plotted against the momentum thickness Reynolds number R_{δ_2} and the enthalpy thickness Reynolds number R_{Δ_2}, respectively. The friction velocities in the APG flows are determined with the method of Nagano et al. (1998). As shown in Fig. 2, the skin friction coefficients decrease drastically in APG flows. The wall heat flux q_w was measured from the mean temperature gradient near the wall, and the Stanton number St was calculated. The measured Stanton number in ZPG flow is well correlated with the correlation curve for a flat plate (Kays and Crawford, 1993). From Fig. 2, it is found that in the APG flows,

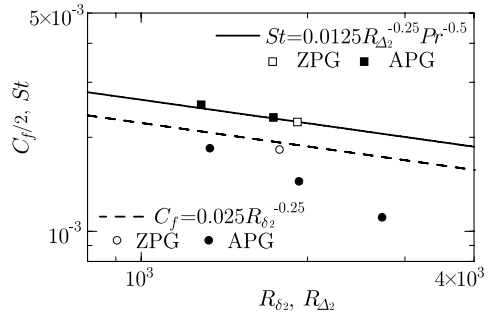

Fig. 2. Skin friction coefficient and Stanton number plotted against momentum thickness Reynolds number and enthalpy thickness Reynolds number.

the Stanton numbers also follow this curve in a fully developed regime.

Fig. 3 shows the mean velocity profiles normalized by the free-stream velocity $\overline{U}/\overline{U}_e$. With increasing P^+, the defect in the mean velocity $\overline{U}$ from the free-stream velocity $\overline{U}_e$ becomes larger. Thus, in the outer coordinates, the mean velocity profile does not maintain self-similarity under the non-equilibrium condition. Fig. 4 shows the mean temperature profiles normalized by the temperature difference between the wall and the ambient, $\overline{\Theta}/\overline{\Theta}_e$. The abscissa is the distance from the wall normalized by the 99% thickness of the thermal boundary layer. As clearly seen from this figure, there are few effects of APG on the

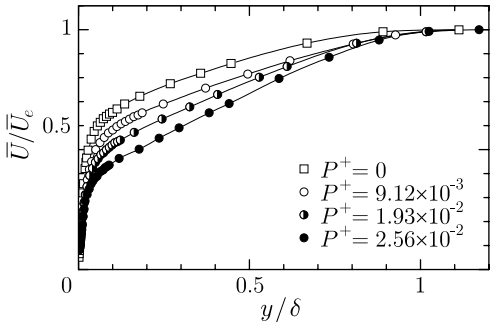

Fig. 3. Mean velocity profiles in ZPG and APG flows in outer coordinates.

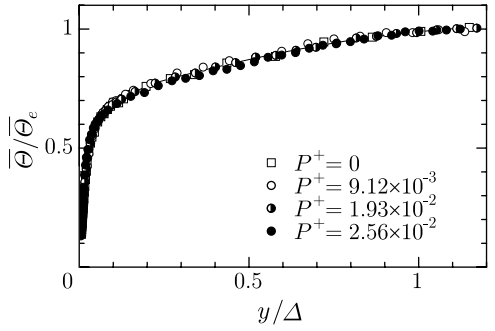

Fig. 4. Mean temperature profiles in ZPG and APG flows in outer coordinates.

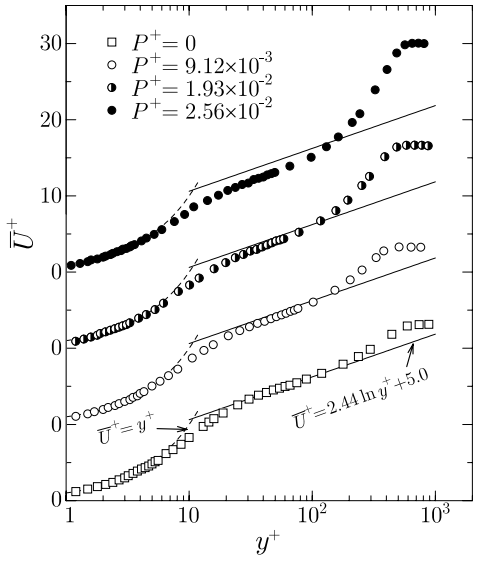

Fig. 5. Mean velocity profiles in ZPG and APG flows in wall coordinates.

mean temperature profiles on the basis of this normalization.

Fig. 5 shows the mean velocity profiles normalized by the friction velocity u_τ. It is clearly seen from this figure that the velocity profiles in APG flows lie below the following "standard" log-law profile for ZPG flows:

$$\overline{U}^+ = 2.44\ln y^+ + 5.0. \tag{1}$$

Moreover, in the outer region, the deviation from the log-law, i.e., the wake component, is very large. Since at the outer edge of the layer, the mean velocity conforms to the free-stream velocity, and is expressed in wall units as $\overline{U}_e^+ = \sqrt{2/C_f}$, the increase in the wake component is due to the significant decrease in the skin friction coefficient (see Fig. 2). These important characteristics of the APG flows conform to our previous results (Nagano et al., 1998), and are also confirmed by direct numerical simulation (DNS) (Spalart and Watmuff, 1993) and actual measurement (Debisschop and Nieuwstadt, 1996).

Fig. 6 shows the mean temperature distribution $\overline{\Theta}$ normalized by the friction temperature θ_τ. In this figure, the broken and solid lines indicate the following respective distributions:

$$\overline{\Theta}^+ = Pry^+, \quad \overline{\Theta}^+ = \kappa_t^{-1}\ln y^+ + C_t, \tag{2}$$

where κ_t and C_t are 0.48 and 3.8 (for $Pr = 0.71$), respectively. In the ZPG flow, the universal log-law region for thermal fields definitely exists as previously reported by many researchers. The turbulent Prandtl number, estimated in the log region, is $Pr_t(=\kappa/\kappa_t) = 0.85$. On the other hand, in the APG flows, the temperature profiles lie below the log-law profile, and the increase disappears in the wake region generally seen in the mean velocity profiles of APG flows (see Fig. 5). These important characteristics of APG flows conform to previously reported experimental results in equilibrium APG flows (Perry et al., 1966; Blackwell

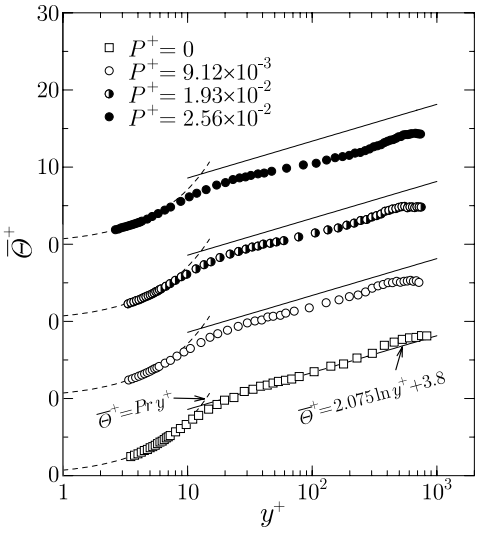

Fig. 6. Mean temperature profiles in ZPG and APG flows in wall coordinates.

et al., 1972) and well correspond to the theoretical conjecture of Bradshaw and Huang (1995), i.e., the law of the wall for a thermal field is more affected by pressure gradient than that for a velocity field. It should be noted that this reduction in the mean temperature at the outer edge of the layer, i.e., $\overline{\Theta}_e^+(=\sqrt{C_f/2}/St)$, is mainly due to the reduction in the skin friction coefficient, because the Stanton number is unchanged by imposing an APG.

Fig. 7 shows the profiles of Reynolds shear stress, $-\overline{uv}$, normalized by the friction velocity, u_τ. The abscissa is the distance from the wall normalized by the 99% thickness of the boundary layer, δ. It includes the experimental and numerical results in ZPG flows (Verriopoulos, 1983; Spalart, 1988). With increasing P^+, $-\overline{uv}/u_\tau^2$ drastically increases in the outer region. Thus, the constant-stress-layer relationship $-\overline{uv}/u_\tau^2 \simeq 1$ observed in the ZPG flows is no longer valid. This, too, may account for the non-existence of the universal law of the wall in APG boundary layers. Fig. 8 shows the wall-normal heat flux, $-\overline{v\theta}$, normalized by the friction velocity, u_τ, and temperature, θ_τ, in ZPG and APG flows. As seen from Fig. 8, the wall-normal heat flux in APG flow is kept unchanged over the entire region compared with Reynolds shear stress in Fig. 7. In our previous experiment (Nagano et al., 1998), the intensity of the wall-normal velocity component, v, normalized by free-stream velocity, $\overline{U}_0$, at the inlet to the test section was not affected. Because the heat transfer is determined with the wall-normal motions, little effect of APG on wall-normal velocity component results in correspondingly little change in the thermal field.

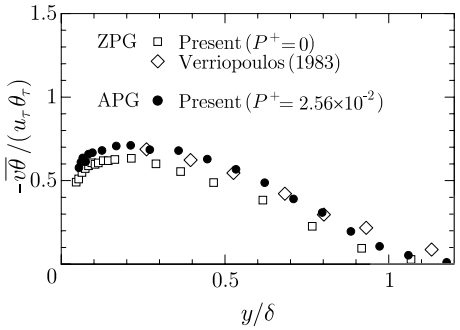

Fig. 8. Wall-normal turbulent heat flux in ZPG and APG flows.

Fig. 9 shows the eddy diffusivities for momentum and heat, ν_t and α_t, respectively, normalized by the free-stream velocity, $\overline{U}_e$, and the displacement thickness, δ_1, defined as

$$\nu_t = \frac{-\overline{uv}}{\partial\overline{U}/\partial y}, \quad \alpha_t = \frac{-\overline{v\theta}}{\partial\overline{\Theta}/\partial y}. \tag{3}$$

As seen in Fig. 9, the eddy diffusivity for the momentum, ν_t, in the APG flow decreases in the large part of the boundary layer ($y/\delta > 0.1$) in comparison with the ZPG flow. On the other hand, because the mean temperature gradient has not been affected, though the wall-normal heat flux is slightly changed, the eddy diffusivity for heat, α_t, results in a small amount of decrease in APG flow in comparison with ZPG flow (see Fig. 9). Thus, as shown in Fig. 10, the turbulent Prandtl number $Pr_t = \nu_t/\alpha_t$ in APG flow decreases in the outer layer ($y/\delta > 0.3$), because the ν_t strongly decreases.

3.2. Fractional contributions

To understand the above features of the APG flows in more detail, we have investigated the fractional

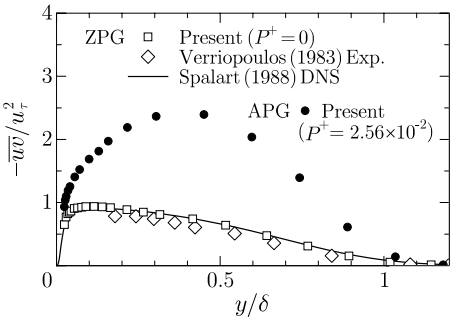

Fig. 7. Reynolds shear stress in ZPG and APG flows.

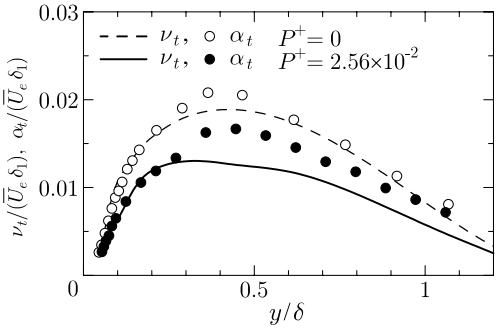

Fig. 9. Eddy diffusivities for momentum and heat in ZPG and APG flows.

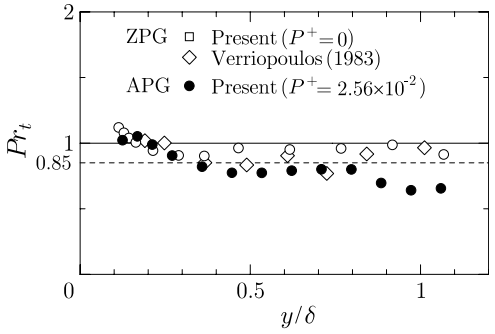

Fig. 10. Turbulent Prandtl number distributions in ZPG and APG flows.

contributions of the coherent motions to Reynolds shear stress, $-\overline{uv}$, and wall-normal turbulent heat flux, $-\overline{v\theta}$, as shown in Figs. 11 and 12, respectively. In the ZPG flow (Figs. 11(a) and 12(a)), Reynolds shear stress and wall-normal heat flux are dominated mainly by the $Q2$- and $Q4$-motions in comparison with the interaction motions $(Q1, Q3)$. Moreover, in the log region the contribution of $Q2$-motions to both Reynolds shear stress and wall-normal heat flux is larger than that of $Q4$-motions. On the other hand, in the APG flow (Figs. 11(b) and 12(b)), the contribution of sweep motions ($Q4$) to Reynolds shear stress $-\overline{uv}$ becomes larger than that of ejection motions ($Q2$) in the log region. However, the contributions to the wall-normal heat flux, $-\overline{v\theta}$, from the ejection motions ($Q2$) and sweep motions ($Q4$) show smaller differences, thus indicating that the effects of the APG on heat transfer are smaller than on momentum transfer.

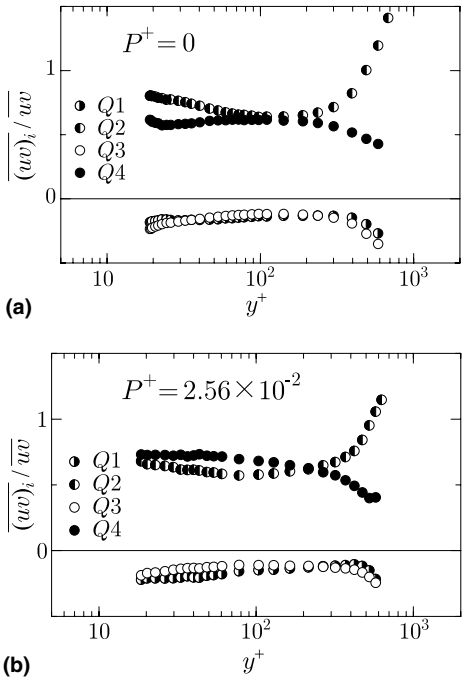

Fig. 11. Fractional contributions to Reynolds shear stress from different motions: (a) $P^+=0$; (b) $P^+=2.56\times10^{-2}$.

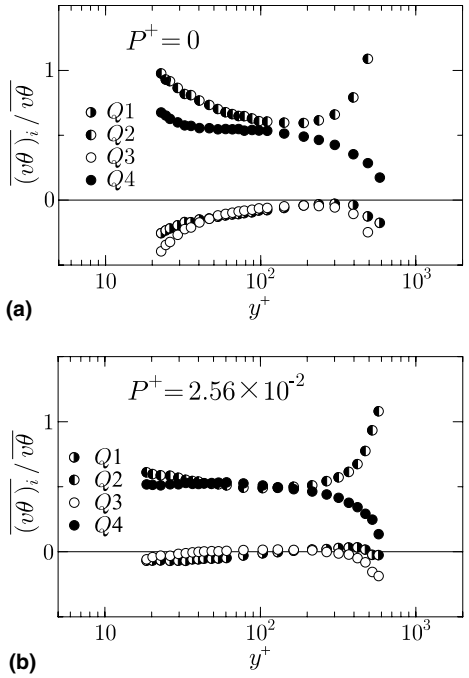

Fig. 12. Fractional contributions to wall-normal heat flux from different motions: (a) $P^+=0$; (b) $P^+=2.56\times10^{-2}$.

3.3. Trajectory analysis

To clarify the changes in coherent motions in APG flows, we have conducted the trajectory analysis developed by Nagano and Tagawa (1995) and extracted the key patterns and flow modules contributing to the momentum and heat transports, which consist of three successive quadrants in the (u,v)-plane. In the log region ($y^+\simeq 50$) of the ZPG and APG flows, the number of detected events and fractional contributions to $-\overline{uv}/u_\tau^2$ and $-\overline{v\theta}/(u_\tau\theta_\tau)$ were evaluated. It was confirmed that the $Q4$–$Q1$–$Q4$ and the $Q2$–$Q3$–$Q2$ patterns occur most frequently, and that they make very large contributions to the Reynolds shear stress and the wall-normal heat flux, irrespective of pressure gradients. These trajectories are called the sub-patterns (Nagano and Tagawa, 1995).

Fig. 13 shows the ensemble-averaged velocity and temperature fluctuations, $\langle\hat{u}\rangle$, $\langle\hat{v}\rangle$ and $\langle\hat{\theta}\rangle$, and its correlations, $-\langle\hat{u}\hat{v}\rangle$, $\langle\hat{u}\hat{\theta}\rangle$ and $-\langle\hat{v}\hat{\theta}\rangle$, of the identified sub-patterns ($Q4$–$Q1$–$Q4$ and $Q2$–$Q3$–$Q2$) in the log region. A caret denotes the normalization by the respective r.m.s. value. The time on the abscissa is normalized by the Taylor time scale τ_E, which is the most appropriate for scaling the period of the coherent motions, irrespective of pressure gradients (Nagano et al., 1998). The mean burst periods have nearly the same value of 10 τ_E in both ZPG and APG flows at this location.

In the ZPG flow, as shown in Fig. 13(a), the amplitude of the $Q2$-motions in the $Q2$–$Q3$–$Q2$ pattern is relatively larger than that of the $Q4$-motions in the $Q4$–$Q1$–$Q4$ pattern for both the velocity and thermal fields. In the APG flow, as shown in Fig. 13(b), the amplitude of the ensem-

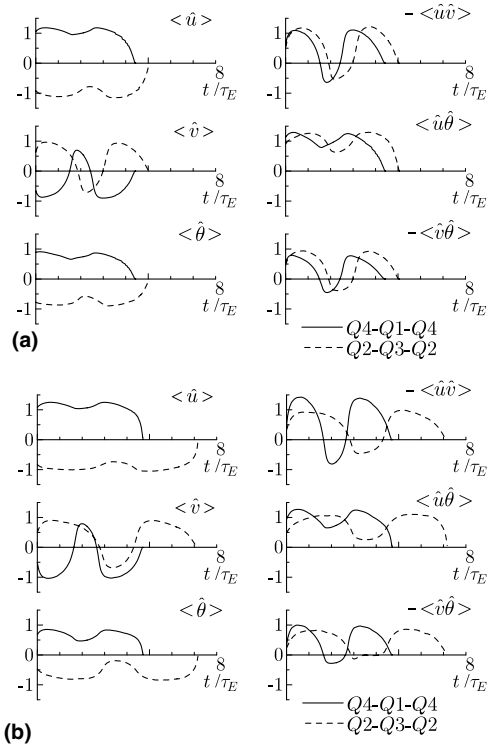

Fig. 13. Ensemble-averaged characteristics of velocity and temperature fluctuations ($Q4$–$Q1$–$Q4$ and $Q2$–$Q3$–$Q2$ patterns) in the log region ($y^+ \simeq 50$): (a) $P^+ = 0$; (b) $P^+ = 2.56 \times 10^{-2}$.

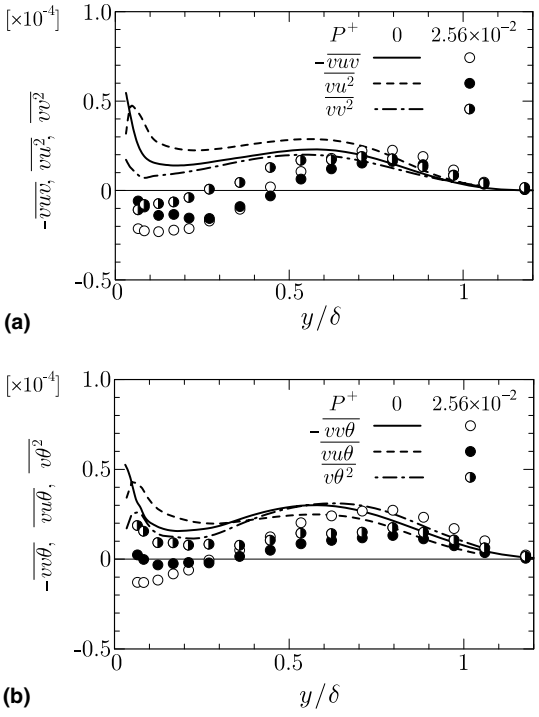

Fig. 14. Distributions of turbulent transport in ZPG and APG flows: (a) velocity field; (b) thermal field. Velocity and temperature fluctuations are normalized by $\overline{U}_0$ and $\overline{\Theta}_e$, respectively.

ble-averaged fluctuations decreases in $Q2$-motions, and the duration of the $Q2$–$Q3$–$Q2$ patterns becomes larger. On the other hand, the amplitude of the $Q4$–$Q1$–$Q4$ pattern becomes larger, but the duration becomes shorter. Moreover, the contribution of $Q4$–$Q1$–$Q4$ to the momentum transfer becomes larger than that of $Q2$–$Q3$–$Q2$ in the APG flow (Houra et al., 2000). For the thermal field, both of the sub-patterns ($Q4$–$Q1$–$Q4$ and $Q2$–$Q3$–$Q2$) contribute to the wall-normal heat flux in the APG flow. Thus, both of these sub-patterns are identified as important flow modules for the heat transfer.

3.4. Turbulent transports

The structural differences in quasi-coherent motions reflect on higher-order turbulent statistics, especially third-order moments (Nagano and Tagawa, 1988). The distributions of turbulent transport in the velocity and thermal fields are presented in Fig. 14(a) and (b), respectively. The definite effects of the APG are clearly seen in the velocity field, i.e., as shown in Fig. 14(a), the positive region of $-\overline{vuv}$, $\overline{vu^2}$, and $\overline{vv^2}$ in the ZPG flows disappears at the inner region as P^+ increases. Since third-order moments are predominately sensitive to the change of coherent structures such as ejections and sweeps (Nagano and Tagawa, 1988), this result indicates that internal structural changes do occur in the velocity field of APG boundary layers. Negative values of $\overline{vu^2}$ in the near-wall to outer regions demonstrate the existence of turbulent energy transport toward the wall from the regions away from the wall. This important characteristic of the APG flows conforms to our previous result (Nagano et al., 1998), and is also consistent with the results of Bradshaw (1967), Cutler and Johnston (1989), Skåre and Krogstad (1994). From Fig. 14(b), it can be seen that a similar inward transfer takes place in the turbulent transport of the thermal field. However, the change in the thermal field is relatively small compared with that in the velocity field.

3.5. Bispectra of turbulent transports

Because the turbulent transports consist of non-linear interactions in the turbulent motions, it is important to investigate these interactions in the Fourier space. The bispectrum is defined as the Fourier transform of the triple moment (Nagano and Houra, 2002). For example, the bispectrum $B_{-vuv}(f_2,f_3)$ of the triple moment $-\overline{vuv}$ is written as follows:

$$B_{-vuv}(f_2,f_3) = \int\int_{-\infty}^{+\infty} -\overline{v(t)u(t+t_2)v(t+t_3)}\,e^{-i2\pi(f_2t_2+f_3t_3)}\,dt_2\,dt_3 \tag{4}$$

and

$$-\overline{v(t)u(t+t_2)v(t+t_3)} = \int\int_{-\infty}^{+\infty} B_{-vuv}(f_2,f_3)\,e^{i2\pi(f_2t_2+f_3t_3)}\,df_2\,df_3. \tag{5}$$

Thus, the bispectrum analyzes the frequency-dependent interactions between the frequency components at f_2, f_3,

and f_2+f_3. If we put $t_2=t_3=0$, the following relation is obtained:

$$-\overline{vuv}=\int\int_{-\infty}^{+\infty}B_{-vuv}(f_2,f_3)\,\mathrm{d}f_2\,\mathrm{d}f_3. \tag{6}$$

In practice, the bispectrum is calculated using the following relation:

$$B_{-vuv}(f_2,f_3)=-\overline{\tilde{v}^*(f_2+f_3)\tilde{u}(f_2)\tilde{v}(f_3)}, \tag{7}$$

where $\tilde{u}(f)$ is the Fourier transform of a velocity fluctuation $u(t)$. An asterisk "*" denotes a complex conjugate. Since the mean transport by turbulent motions is expressed in real values, we discuss the real part of the measured bispectrum. The time-series data analyzed are real values, and so the bispectra are symmetric at the origin in the (f_2,f_3)-plane. Thus, half of (f_2,f_3)-plane is sufficient to describe the bispectrum.

Figs. 15 and 16 show the measured bispectra, $B_{-vuv}(f_2,f_3)$, of the turbulent transport of the Reynolds shear stress, $-\overline{vuv}$, and the bispectra, $B_{-vv\theta}(f_2,f_3)$, of the turbulent transport of the wall-normal heat flux, $-\overline{vv\theta}$, respectively, in the ZPG flow ($y/\delta\simeq 0.2$). In a similar way, Figs. 17 and 18 show the measured bispectra, $B_{-vuv}(f_2,f_3)$ and $B_{-vv\theta}(f_2,f_3)$, respectively, in the APG flows ($y/\delta\simeq 0.2$). The left figures, labeled (a), show the sum–frequency interaction $f_1=f_2+f_3$, i.e., non-linear interaction between $\tilde{v}(f_2+f_3)$, $\tilde{u}(f_2)$ and $\tilde{v}(f_3)$ in Figs. 15 and 17. On the other hand, the right figures, labeled (b), show the difference–frequency interaction $f_1=|f_2|-|f_3|$, i.e., non-linear interaction between $\tilde{v}(|f_2|-|f_3|)$, $\tilde{u}(f_2)$ and $\tilde{v}(f_3)$ in

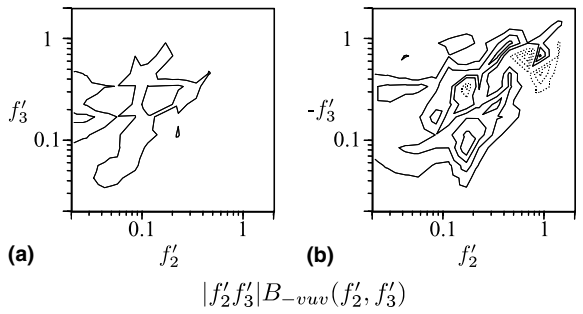

Fig. 15. Bispectra of $-vuv$ in ZPG flow ($y/\delta\simeq 0.2$): (a) sum–frequency interaction; (b) difference–frequency interaction.

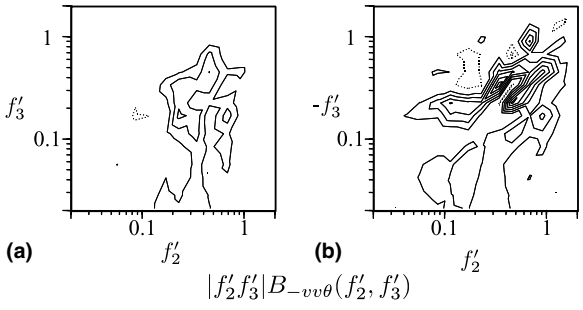

Fig. 16. Bispectra of $-vv\theta$ in ZPG flow ($y/\delta\simeq 0.2$): (a) sum–frequency interaction; (b) difference–frequency interaction.

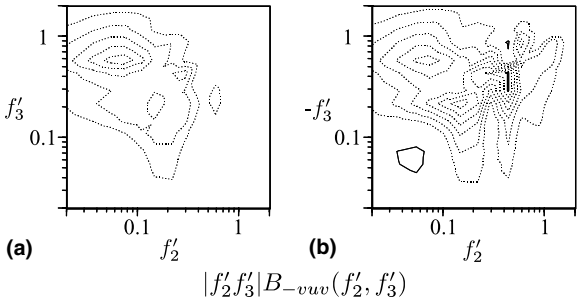

Fig. 17. Bispectra of $-vuv$ in APG flow ($y/\delta\simeq 0.2$): (a) sum–frequency interaction; (b) difference–frequency interaction.

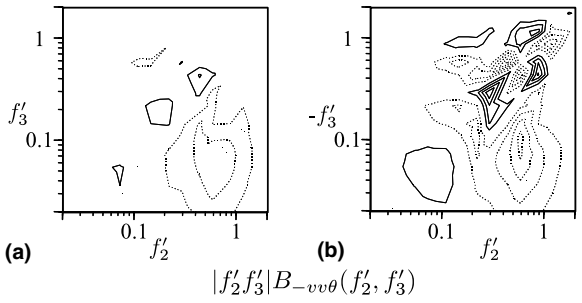

Fig. 18. Bispectra of $-vv\theta$ in APG flow ($y/\delta\simeq 0.2$): (a) sum–frequency interaction; (b) difference–frequency interaction.

Figs. 15 and 17. Because we need to show the net contribution to the bispectra on the frequency axes at the log-scale, the bispectra multiplied by frequencies, e.g., $|f_2f_3|B_{-vuv}(f_2,f_3)$, are shown. The frequencies in the axes are normalized by the Taylor time scale, $f'=f\tau_{\mathrm{E}}$. The normalized frequency of the bursting events in the near-wall region corresponds to about 0.1 (Nagano et al., 1998). In the figures, the measured bispectra are normalized by the absolute maximum value. The solid and broken contour lines, respectively, show positive and negative values, and the interval between successive contour lines is 0.1.

In the ZPG flow, strong positive regions for the difference–frequency interactions in both velocity and thermal fields (Figs. 15(b) and 16(b)) are seen along the same frequency, i.e., on the diagonal line of the (f_2,f_3)-plane over the frequency range from 0.1 to 1.0, and the positive values ($B_{-vuv}>0$ and $B_{-vv\theta}>0$) indicate that non-linear transport from the wall to the outer regions is dominant. In Figs. 15(a) and 16(a), slight positive regions are discernible within the low frequencies; however, the transport associated with the sum–frequency interaction is very small.

For the velocity field in the APG flow, as seen in Fig. 17, the streamwise fluctuating velocity $\tilde{u}(f_2')$ with low frequency $f_2'\simeq 0.06$ and the wall-normal fluctuation $\tilde{v}(f_3')$ with high frequency $f_3'\simeq 0.6$ interact with both $\tilde{v}(f_2'+f_3')$ and $\tilde{v}(|f_2'|-|f_3'|)$. This non-local interaction results in the wallward turbulent transfer ($B_{-vuv}<0$). Moreover, this negative contribution to the bispectra corresponds to the sweep motions associated with high-frequency wall-normal fluctuations ($Q4$–$Q1$–$Q4$ pattern) in the near-wall region of

the APG flow. A similar wallward transfer ($B_{-vv\theta} < 0$) with high-frequency wall-normal velocity fluctuation $\tilde{v}(f_2' \simeq 0.6)$ is observed for the thermal field in the APG flow (Fig. 18). However, along the diagonal line of the (f_2,f_3)-plane over the higher frequency range $(f_2' \simeq f_3' > 0.2)$, both positive and negative contributions are seen in Fig. 18. Thus, for the thermal field, the turbulence transport is fairly complex.

4. Conclusions

Experimental investigation has been made on non-equilibrium turbulent boundary layers subjected to adverse pressure gradients developing on the uniformly heated flat wall. The results can be summarized as follows:

1. In the APG boundary layer, the Stanton number follows the correlation curve for a flat plate, although the skin friction coefficient decreases drastically in comparison with ZPG flow. The conventional thermal law of the wall does not hold in the fully turbulent region. Moreover, turbulent Prandtl number decreases in the fully turbulent region, i.e., the eddy diffusivity for heat becomes much larger than that for momentum.
2. The quadrant splitting and trajectory analyses reveal that the effects of APG on the thermal field are not similar to those on the velocity field. Both the ejection- and sweep-motions contribute significantly to the heat transport in the APG flow, though the sweep motions whose durations become shorter are the main contributors to the momentum transfer.
3. In the APG flow, the turbulent transports for the momentum and heat occur in the direction toward the wall from the region away from the wall. The structural change in APG flow causes the non-local interactions between the temperature fluctuations and the wall-normal motions. The situation is fairly complex.

Acknowledgement

This work was partially supported by a Grant-in-Aid for Scientific Research (S) (No. 17106003) from the Ministry of Education, Culture, Sports, Science and Technology (MEXT).

References

Blackwell, B.F., Kays, W.M., Moffat, R.J., 1972. The turbulent boundary layer on a porous plate: an experimental study on the heat transfer behavior with adverse pressure gradients. Thermosciences Division, Department of Mechanical Engineering, Stanford University, Report HMT-16, Stanford, CA.

Bradshaw, P., 1967. The turbulence structure of equilibrium boundary layers. J. Fluid Mech. 29, 625–645.

Bradshaw, P., Huang, P.G., 1995. The law of the wall in turbulent flow. Proc. R. Soc. Lond. A 451, 165–188.

Clauser, F.H., 1954. Turbulent boundary layers in adverse pressure gradients. J. Aero. Sci. 21, 91–108.

Coleman, G.N., Kim, J., Spalart, P.R., 2003. Direct numerical simulation of a decelerated wall-bounded turbulent shear flow. J. Fluid Mech. 495, 1–18.

Cutler, A.D., Johnston, J.P., 1989. The relaxation of a turbulent boundary layer in an adverse pressure gradient. J. Fluid Mech. 200, 367–387.

Debisschop, J.R., Nieuwstadt, F.T.M., 1996. Turbulent boundary layer in an adverse pressure gradient: effectiveness of riblets. AIAA J. 34, 932–937.

Fernando, E.M., Smits, A.J., 1990. A supersonic turbulent boundary layer in an adverse pressure gradient. J. Fluid Mech. 211, 285–307.

Hishida, M., Nagano, Y., 1978. Simultaneous measurements of velocity and temperature in nonisothermal flows. Trans. ASME J. Heat Transfer 100, 340–345.

Hishida, M., Nagano, Y., 1988a. Turbulence measurements with symmetrically bent V-shaped hot-wires. Part 1: principles of operation. Trans. ASME J. Fluid Eng. 110, 264–269.

Hishida, M., Nagano, Y., 1988b. Turbulence measurements with symmetrically bent V-shaped hot-wires. Part 2: measuring velocity components and turbulent shear stresses. Trans. ASME J. Fluid Eng. 110, 270–274.

Houra, T., Tsuji, T., Nagano, Y., 2000. Effects of adverse pressure gradient on quasi-coherent structures in turbulent boundary layer. Int. J. Heat Fluid Flow 21, 304–311.

Kays, W.M., Crawford, M.E., 1993. Convective Heat and Mass Transfer, third ed. McGraw-Hill, New York.

Lu, S.S., Willmarth, W.W., 1973. Measurements of the structure of the reynolds stress in a turbulent boundary layer. J. Fluid Mech. 60, 481–511.

Na, Y., Moin, P., 1996. Direct numerical simulation of turbulent boundary layers with adverse pressure gradient and separation. Stanford University Report TF-68.

Nagano, Y., Houra, T., 2002. Higher-order moments and spectra of velocity fluctuations in adverse-pressure-gradient turbulent boundary layer. Exp. Fluids 33, 22–30.

Nagano, Y., Tagawa, M., 1988. Statistical characteristics of wall turbulence with a passive scalar. J. Fluid Mech. 196, 157–185.

Nagano, Y., Tagawa, M., 1995. Coherent motions and heat transfer in a wall turbulent shear flow. J. Fluid Mech. 305, 127–157.

Nagano, Y., Tsuji, T., 1994. Recent developments in hot- and cold-wire techniques for measurements in turbulent shear flows near walls. Exp. Therm. Fluid Sci 9, 94–110.

Nagano, Y., Tagawa, M., Tsuji, T., 1993. Effects of adverse pressure gradients on mean flows and turbulence statistics in a boundary layer. In: Durst, F., Friedrich, R., Launder, B.E., Schmidt, F.W., Schumann, U., Whitelaw, J.H. (Eds.), Turbulent Shear Flows, vol. 8. Springer-Verlag, Berlin, pp. 7–21.

Nagano, Y., Tsuji, T., Houra, T., 1998. Structure of turbulent boundary layer subjected to adverse pressure gradient. Int. J. Heat Fluid Flow 19, 563–572.

Perry, A.E., Bell, J.B., Joubert, P.N., 1966. Velocity and temperature profiles in adverse pressure gradient turbulent boundary layer. J. Fluid Mech. 25, 299–320.

Rotta, J.C., 1962. Turbulent boundary layers in incompressible flow. Prog. Aero. Sci. 2, 1–221.

Samuel, A.E., Joubert, P.N., 1974. A boundary layer developing in an increasingly adverse pressure gradient. J. Fluid Mech. 66, 481–505.

Skåre, P.E., Krogstad, P.-Å., 1994. A turbulent equilibrium boundary layer near separation. J. Fluid Mech. 272, 319–348.

Spalart, P.R., 1988. Direct simulation of a turbulent boundary layer up to $R_\theta = 1410$. J. Fluid Mech. 187, 61–98.

Spalart, P.R., Watmuff, J.H., 1993. Experimental and numerical study of a turbulent boundary layer with pressure gradients. J. Fluid Mech. 249, 337–371.

Spina, E.F., Smits, A.J., Robinson, S.K., 1994. The physics of supersonic turbulent boundary layers. Annu. Rev. Fluid Mech. 26, 287–319.

Stoke, M., Henningson, D.S., Henkes, R.A.W.M., 1998. Direct numerical simulation of self-similar turbulent boundary layers in adverse pressure gradients. Flows, Turbul. Combust. 60, 47–85.

Tagawa, M., Tsuji, T., Nagano, Y., 1992. Evaluation of X-probe response to wire separation for wall turbulence measurements. Exp. Fluids 12, 413–421.

Townsend, A.A., 1976. The Structure of Turbulent Shear Flow, second ed. Cambridge University Press, Cambridge.

Verriopoulos, C.A., 1983. Effects of convex surface curvature on heat transfer in turbulent flow. Ph.D. Thesis, Imperial College.

Volino, R.J., Simon, T.W., 1997. Velocity and temperature profiles in turbulent boundary layer flows experiencing streamwise pressure gradients. Trans. ASME J. Heat Transfer 119, 433–439.